Available online at www.sciencedirect.com
ScienceDirect
Ceramics International 37 (2011) 223–230
CERAMICS INTERNATIONAL
www.elsevier.com/locate/ceramint

Preparation of porous SiC ceramics by an infiltration technique

Atanu Dey, Nijhuma Kayal, Omprakash Chakrabarti *

Central Glass and Ceramic Research Institute, (Council of Scientific and Industrial Research) 196, Raja S. C. Mullick Road, Kolkata 700 032, India

Received 18 April 2010; received in revised form 15 May 2010; accepted 23 August 2010
Available online 29 September 2010

Abstract:

The possibility of infiltration as a technique for synthesizing porous SiC ceramics was examined. SiC powder compacts were infiltrated with a liquid precursor which produced SiO_2 during pyrolysis in air at a low temperature. Infiltrated SiO_2 might act as a bond between the neighboring SiC particles at contacting points. The process parameters which control the rate of infiltration of liquid precursor to SiO_2 into porous SiC powder compacts were studied. Results showed that the infiltration rate could be estimated by using weight gain measurements. Sintering infiltrated bodies at 1300 °C yielded specimens in which only silicon carbide and cristobalite were detected. The presence of cristobalite significantly controlled the porosity as also the mechanical properties. Reasonable flexural strengths (∼ 48 MPa) could be achieved at a porosity level of 26 vol.% with near uniform pore diameter of around 5 μm.
© 2010 Elsevier Ltd and Techna Group S.r.l. All rights reserved.

Keywords: SiC Ceramics; Porous material; Infiltration; Silica sol

1. Introduction

Currently, porous SiC ceramics have been a focus of interesting research in the field of porous materials due to their excellent structural properties, high strength, high hardness, and superb mechanical and chemical stabilities, particularly at high temperatures and hostile atmospheres. Porous SiC ceramics have been considered as suitable candidate materials for catalyst supports [1,2], hot gas or molten metal filters [3], high temperature membrane reactors [4], thermal insulating materials [5], gas sensors [6] etc. Porous SiC ceramics are fabricated by various methods including partial sintering [7], carbothermal reduction [8,9], replication or pyrolysis of polymeric sponge [10–12], reaction bonding [13,14] etc. In all these methods SiC needs to be sintered which requires a very high temperature due to the strong covalent nature of the Si–C bond, selective sintering additives, expensive atmosphere, costly equipment and delicate instrumentation. Processing of porous SiC ceramics at low temperature using a simple technique thus becomes necessary. In order to realize the low temperature fabrication of porous SiC ceramics She et al. [15] developed an oxidation bonding technique in which porous powder compact of SiC was heat treated in air to promote oxidation and consequently to bind SiC particles by oxidation derived SiO_2 glass. The author used graphite as a pore former [16]. The mechanical behavior of the oxidation bonded SiC was further improved by addition of fine alumina powder which could react with silica with in situ formation of strong mullite bond [17]. Ding et al. [18] also reported formation of porous mullite bonded SiC ceramics following identical procedure and using a powder compact of SiC and Al_2O_3 formed by dry pressing. Bardhana et al. followed colloidal processing route to prepare SiC ceramics bonded with mullite formed in situ [19]. Liu et al. [20] investigated on in situ formation of cordierite for application as bonds in porous SiC ceramics. Oxide bonding of porous SiC ceramics of honeycomb structure has been reported by Morimoto et al. in which external addition of cordierite was made as a secondary bond phase [21]. Although all these methods are successful in forming oxide bond for porous SiC ceramics, they suffer from many shortcomings. For example, oxidation bonding of SiC is limited in the depth of the zone which can be oxidized and is therefore not practical for large scale production. Mechanical mixing of silicon carbide and alumina powders followed by heat treatment can result in bodies containing flaws due to inhomogeneous mixing. Traditional colloidal powder processing methods, while mixing the SiC and alumina powders in suspension, are often time

* Corresponding author. Tel.: +91 33 2473469/3496x3473; fax: +91 33 24730957.
E-mail address: omprakash@cgcri.res.in (O. Chakrabarti).

0272-8842/$36.00 © 2010 Elsevier Ltd and Techna Group S.r.l. All rights reserved.
doi:10.1016/j.ceramint.2010.09.022

consuming, requiring careful control over the suspension rheology. This paper presents the results of a study on the processing of silica bonded porous SiC ceramics using a liquid infiltration technique. Green SiC specimen produced from SiC powder was infiltrated with a liquid polymer precursor of silica (ethyl silicate). Hydrolyzed ethyl silicate decomposed to SiO_2 at low temperatures which acted as a bond for SiC particles and led to production of a porous ceramics. Two parameters which are available for controlling the infiltration process in this system are time and the chemistry of the polymeric silica sol. Tetraethylorthosilicate (TEOS) was used as the precursor of silica which underwent hydrolysis and polycondensation reactions and eventually led to gelation. For the present work, only the time was controlled to regulate the depth of the infiltration. Finally the properties of silica-bonded porous SiC ceramics (SBSC) synthesized via this infiltration route and the normal oxidation bonding method were compared.

2. Experimental

A commercially available α-SiC powder (M/S Grindwell Norton, India; SiC 98.20%, free carbon 0.25%, SiO_2 0.50%, Fe_2O_3 0.04% w/w) was used in this work. The particles were of irregular shape with non-uniform distribution of size (Fig. 1). The particle size of SiC powder was determined by Malvern laser particle size analyzer (MASTERSIZER 2000 MU, UK). The d_{10}, d_{50} and d_{90} were found to be 9.48, 22.48 and 43.11 μm respectively. SiC powder was mixed with 10% solution of polyvinyl alcohol (Loba Chemie, India; 10 wt.% PVA in water). The mixture was kneaded well to develop suitable workability for compaction and was pressed at 23 MPa pressure in a stainless steel die. The green specimens (50 mm × 20 mm × 16 mm) were dried in an air oven for 24 h at 100 °C and the dimensional measurement and weights were taken.

A silica sol was prepared by mixing 11 ml of 0.1 N HCl with 37 ml of tetraethyl ortho silicate, TEOS, (98%, Acros Organics, NJ, USA) under vigorous mixing for 30 min; the ultimate pH was adjusted in the range of 1.6–1.7. The sol was characterized by measurement of viscosity with a rotational viscometer (HAAKE Instrument, VT 500, Germany). The sol particle size was determined as a function of time by dynamic light scattering (DLS) technique (Zetasizer, ZEN 3600, Malvern, USA) and the thermal decomposition behavior of silica precursor gel was examined by performing thermogravimetric analysis (STA 490C, Netzcsh-Geratebau, GambH, Germany) at a heating rate of 10 °C/min in air up to 1400 °C.

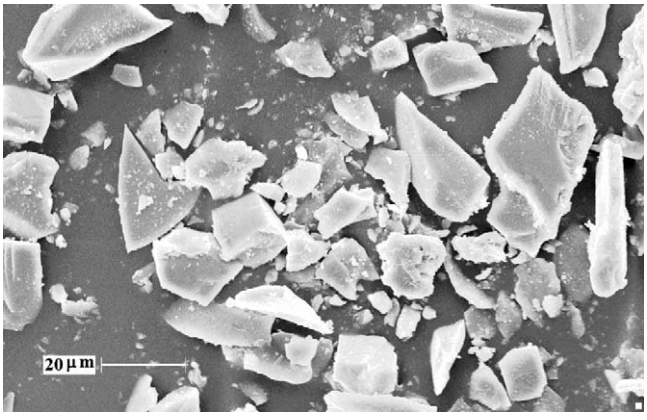

Fig. 1. SEM photomicrograph of α-SiC particles showing variation in sizes.

To determine the suitable infiltration conditions, a preliminary investigation was conducted on powder compacts. A representative sample (18 mm × 20 mm × 16 mm) was cut from the pressed bar, dried at 100 °C for 2 h, suspended in the silica sol by an wire attached to an electric balance (Metler PE 400, USA) and its weight was recorded as a function of time. After the infiltration was complete, the density of the silica sol was determined by weighing a known volume. Knowing the sol density and the mass increase during infiltration, the infiltration volume was plotted as a function of time. Infiltration measurements conditions where the powder compact was evacuated of air were performed by placing the well-dried specimen in a vacuum desicator and evacuating at a vacuum of 40 Pa for 2 h. After evacuation the sample was taken out and suspended in silica sol for measurement of infiltrated volume as a function of time. In separate experiments the pressed bars were also dried at 100 °C for 2 h, evacuated for 2 h at 40 Pa vacuum and infiltrated with silica sol. The infiltrated samples were dried for 18 h to evaporate the sol solvent and the process was repeated. The increase in mass due to SiO_2 intake was determined and expressed in terms of SiO_2 relative to mass of the initial pressed bar (% of mass increase) to assess infiltration behavior under repetitive conditions. The infiltrated samples were fired at 1300 °C for 4 h in air in alumina tube furnace (TE-3499, Therelek Engineers Pvt. Ltd., Bangalore, India) with a programmed heating and cooling of 10 °C/min.

The final ceramics were characterized by measurement of density by water displacement method (Archimedes method), porosity by boiling water method, identification of crystalline phases by XRD analysis (PW1710, Philips, Holland) using Cu Kα radiation of wave length λ = 1.5406 Å, pore size distribution by Hg-intrusion porosimetry (Poremaster, Quantachrome Instruments Inc., FL, USA). The room temperature flexural strength was determined in three-point mode (with a span of 40 mm, speed of 0.5 m/min, sample cross-section of 4.75 mm × 3.25 mm; samples were ground and polished up to 10 μm finish and tensile surfaces were champhered) using an Instron Universal Testing machine. The deflection was monitored through a LVDT with a resolution of 0.05% of full scale deflection and from the load-deflection data, the Young's modulus was automatically obtained with the help of standard software. Microstructure was examined by scanning electron microscopic (SEM) technique (SE-440, Leo-Cambridge, Cambridge, UK).

3. Results and discussion

3.1. Preparation of SiC powder compacts and silica sol

The relative density of the SiC powder compacts was 0.49. The mercury intrusion porosimetry results in Fig. 2 showed that the powder compact had a monomodal pore size distribution

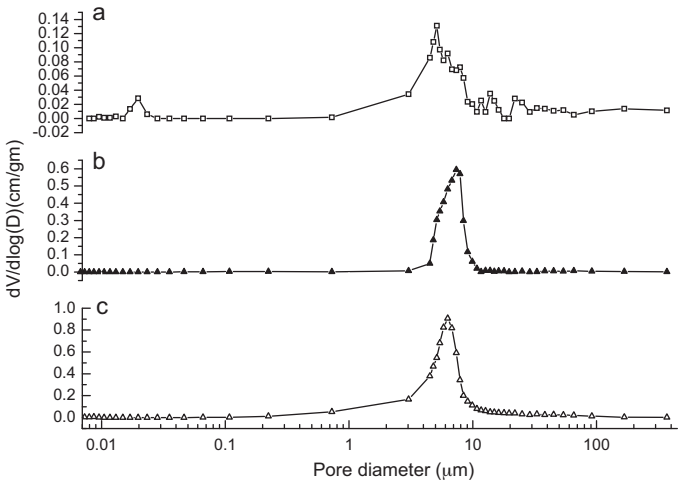

Fig. 2. Pore size distribution patterns measured by Hg-intrusion porosimetry method for green SiC compacts and SBSC ceramics made thereof (a) porous SiC with infiltrated SiO_2 bond phase, (b) porous SiC without infiltrated SiO_2 bond phase and (c) green SiC compact.

varying in the range of 4–8 μm, with peak at pore diameters of 6.32 μm and average pore diameter of 5.90 μm and an average porosity of 50.90 vol.%. This may be due to the wide distribution of SiC particle sizes (Fig. 1). If pores are considered as inclusions randomly distributed in to a volume made of SiC particles and if the pores are assumed to be identical spheres, the minimum inclusion volume needed for formation of a continuous network of pores is reported to be around 16–22% [22,23]. It appears that all the pores in the pressed bars were interconnected forming an open porous network. The size of the starting SiC powders is reflected in the pore size distribution of the green compacts. The formation of continuous porous network may give unhindered and uniform access of the infiltrating liquid into the powder compact.

Acid-catalysed reaction hydrolysis and polycondensation reaction is Eq. (1), represented by

$$Si(OC_2H_5)_4 + H_2O = Si(OH)_4 + 4C_2H_5OH \quad (1)$$

was used for formation of silica sol. The TEOS:water:acid molar ratio and pH are considered important for stability of silica sol. Strong mineral acids were shown to produce positive catalytic effect yielding clear sol with water: TEOS molar ratio > 3 but ≤ 4 [24]. In the present study HCl was used as catalyst and molar composition for generation of clear sol was TEOS:water:acid = $1:3.68:1.1 \times 10^{-3}$ with pH of the acid mixture being adjusted to 1.61. The mixture of TEOS, water and acid was initially found to be biphasic. It transformed to monophasic liquid on stirring for 30 min. At the low pH used in the present study complete hydrolysis was expected [25]. The sol was transparent with no appearance of cloudiness and contained 21.88% (w/w) SiO_2 on theoretical basis. The colloid particles of sol exhibited multimodal size distribution with three major peaks of 42%, 26% and 21% intensities at 4 nm, 29 nm and 1.1 μm particle diameter respectively (Fig. 3). The average particle diameter was found to be 54 nm. It appears that the sol particles were significantly smaller in comparison to the pore diameter of the pressed green bars. Silica sol exhibited perfect shear thinning behavior evident from the linear plot of log (viscosity) versus log shear rate with negative slope (Fig. 4).

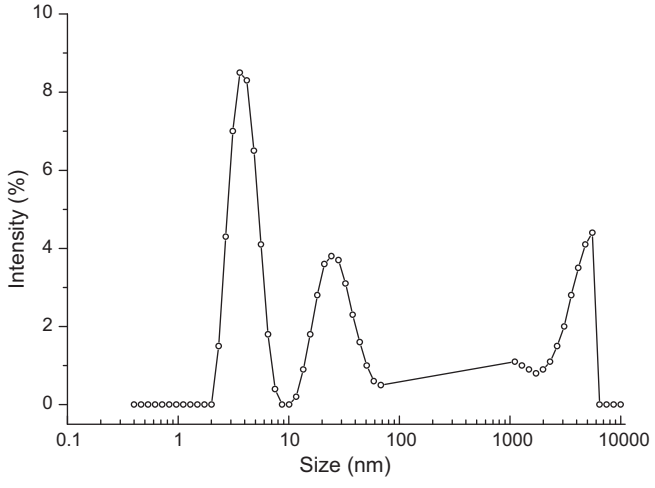

Fig. 3. Particle size distribution pattern of silica sol.

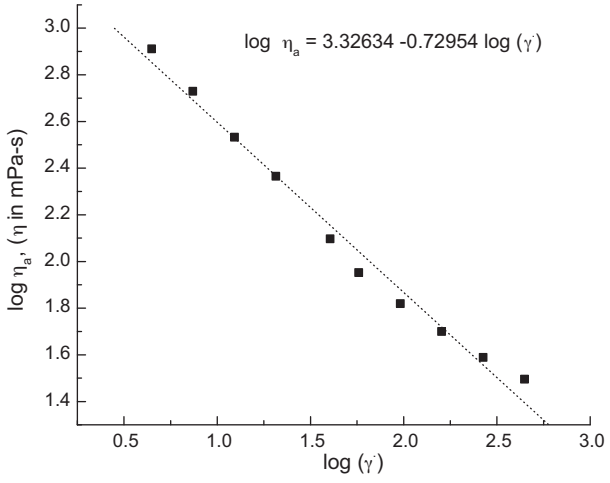

Fig. 4. Characteristics of silica sol precursor— linear plot of log (viscosity,η) versus log(shear rate, γ) indicating shear thinning behaviour of silica sol.

For infiltration purpose SiO_2 sol must be fluid enough to enter and fill the entire void space of the compact and subsequently regain enough viscosity under static condition to remain in the compact. The results of the rheological studies also revealed that the viscosity was low (0.1 Pas) when a high shear rate was applied, but it became high (2.3 Pas) when the shear rate was low, indicating that the sol possesses viscosity with a pronounced shear thinning behavior and was, thus, suitable for infiltration purpose.

3.2. Silica sol infiltration into SiC powder compact

Representative infiltration data for SiC powder compacts evacuated or containing air are represented in Fig. 5; in each case infiltrated volume is plotted against square root of time ($t^{1/2}$). As illustrated in both the cases, the infiltration curves are characterized by similar trends-following a rapid infiltration, the initial linear region departs smoothly to another linear region. Infiltration and flow of liquids through porous media has been well characterized and documented [26,27]. According to these reports infiltration occurs by two different mechanisms. Initially the liquid flow into a porous medium is governed by a capillary pressure and can be described by Eq. (2), following Darcy's law [28].

$$h = \left[\frac{2KP}{\eta}\right]^{1/2} t^{1/2} \quad (2)$$

where h is the distance of the liquid infiltrated in time t, K is the permeability of the porous medium, η is the viscosity and P is the pressure differential which equals to capillary pressure plus any applied pressure minus opposing internal pressure. In absence of any applied pressure capillary pressure causes the wetting liquid to flow into the porous medium until the opposing pressure of the compressed air becomes equal to the capillary pressure. In the later stage the compressed air can diffuse through the liquid and the expression for air diffusion (and thus the concurrent displacement of air by the liquid) is given by Eq. (3), following Ficks law [29]:

$$h = [2D\beta P_a]^{1/2} t^{1/2} \quad (3)$$

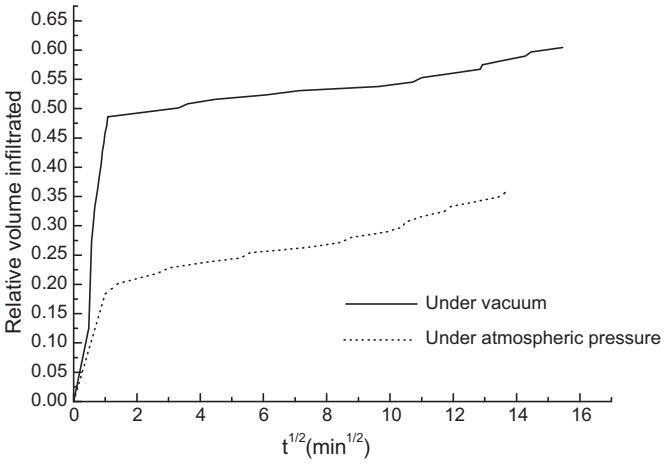

Fig. 5. Time dependence of silica sol infiltration into SiC powder compact.

where, h is the distance of the liquid infiltration with a period of time t, D is the diffusion coefficient of air, β is the Henry's constant and P_a is the pressure of the compressed air. Both the phenomena are concurrent; but the flow of liquid due to capillary pressure initially dominates whereas once the air within the compact is sufficiently compressed, air diffusion dominates. The parabolic behavior of infiltration of silica sol in the powder compacts is supported by the linear infiltration curves obtained in the present study. The capillary infiltration rate constants in case of compacts evacuated and containing air were found to be 3.84×10^{-3} and $3.75 \times 10^{-4}\ s^{-1}$, respectively. In case of evacuated compact the infiltration rate is one order of magnitude higher compared to the compact containing air. It appears to be related to the effect of applied pressure originating from the difference in pressure existing in the pore interior and the outside atmosphere. In the later stage diffusion of air in sol is mainly responsible for infiltration resulting in significantly lower value of infiltration rate constant of $1.67 \times 10^{-6}\ s^{-1}$.

Preliminary investigation indicated that it was not possible to accumulate appreciable amount of silica into a powder compact following a single pass infiltration even for a long period of time. Hence multipass infiltration was performed in order to load silica into the compact to a nearly constant level. Each infiltration cycle consisted of an infiltration under vacuum followed by drying at 100 °C for 18 h. The infiltration time was selected on the basis of the preliminary infiltration investigation result. Representative infiltration weight gain data are summarized in Fig. 6. As expected mass % increase due to silica accumulation was found to increase with number of infiltration pass. The percentage mass increase after fourth infiltration recorded very small increase likely because of the clogging of infiltration channels.

3.3. Effects of infiltrated SiO_2

The thermo gravimetric curve (Fig. 7(a)) of silica gel precursor indicates a three step decomposition involving weight losses due to removal of adsorbed water, decomposition of

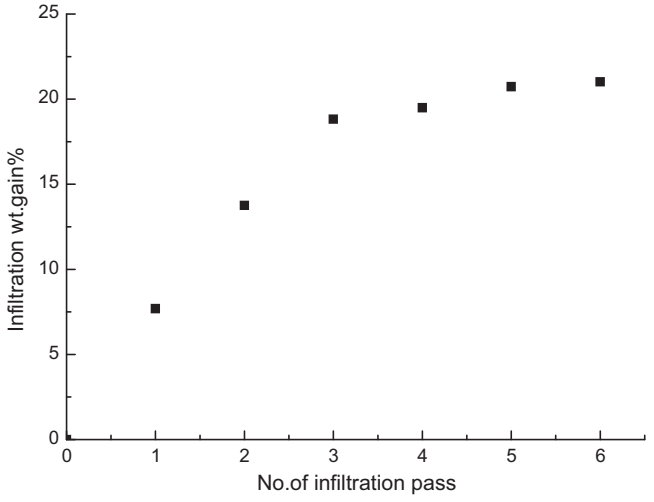

Fig. 6. Effect of infiltration cycle on the amount of accumulated silica in SiC powder compact.

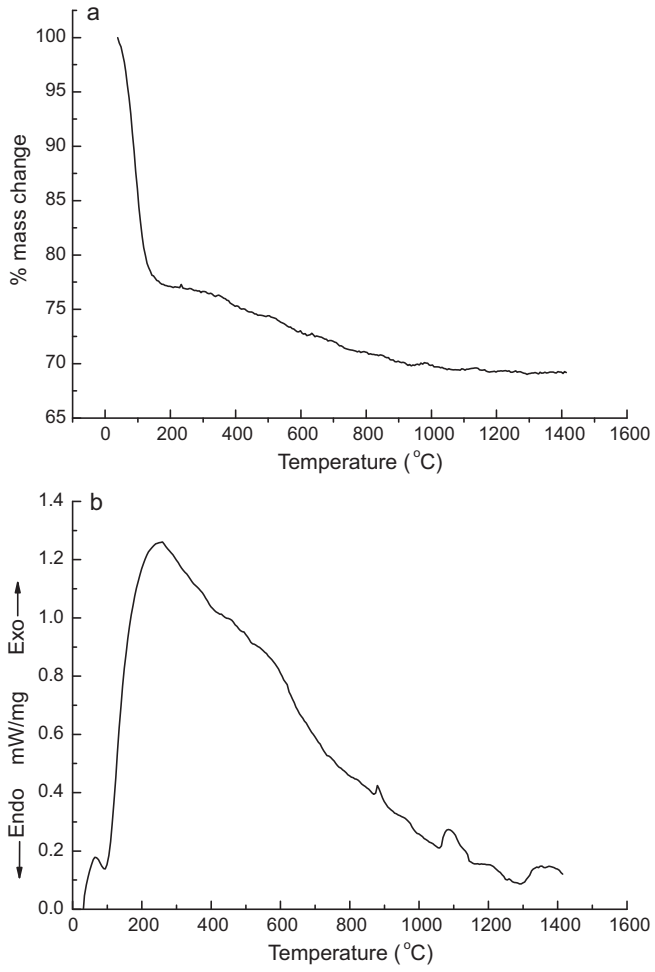

Fig. 7. Response of silica precursor gel during heating up to 1400 °C in air with a heating rate of 10 °C per min. (a) TG- and (b) DTA curves.

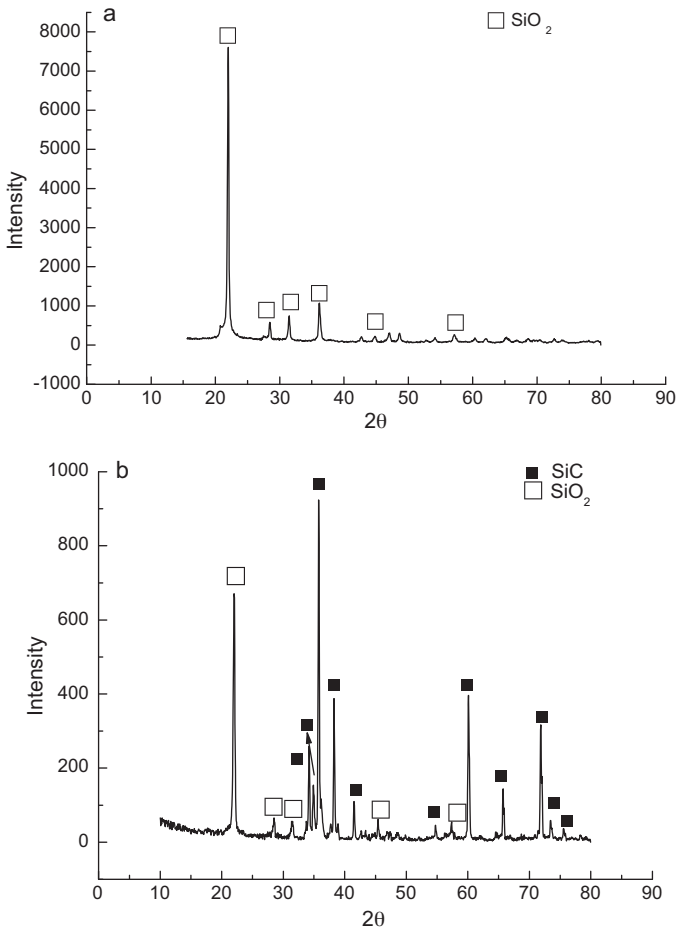

Fig. 8. XRD patterns of (a) Silica precursor gel and (b) silica infiltrated SiC compact heat treated at 1300°C.

organic solvent and an escape of chemically bound water. The accompanying DTA curve (Fig. 7(b)) shows a small endothermic peak at around 100 °C. It might be due to the vaporization and desorption of adsorbed water and release of ethanol (b.p = 78 °C) from the surface of SiO_2 gel [30]. The major decomposition peak is supported by an exothermic transition with a broad peak at around 240 °C. TGA data were similar to those reported by other authors for decomposition of oxide precursor gels synthesized following alkoxide route [31]. Then there is a gradual weight loss up to 1000 °C which could be due to decomposition of organic compounds with elimination of bounded water [32]. A small and broad exothermic peak starting at around 1325 °C might be due to crystallization of cristobalite [32]. The small exothermic peak observed at 1100 °C was likely due to formation of an ultra-structure prior to crystallization of cristobalite. Such behaviour was also observed by other authors in case of formation of cristobalite crystalline phase using alkoxide precursor [33]. Progress of crystallization was expected to occur at 1300 °C with an increase in hold time. XRD-pattern of oxide precursor gel heat treated at 1300 °C for 4 h showed signature peaks of well-developed cristobalite crystallite (Fig. 8(a) and could provide direct proof of this point. The TG and XRD results led to the determination of suitable heat treatment conditions. In order to keep a low processing temperature, silica infiltrated SiC powder compacts were heat treated at 1300 °C with a holding time of 4 h to yield the porous silica bonded SiC (SBSC) ceramic.

Representative data for oxidation weight gain, density, porosity and flexural strength of silica bonded SiC ceramics (SBSC) are summarized in Table 1. Table 1 also consists of similar set of properties of SiC ceramics processed without infiltrated silica. Oxidation of SiC particles caused gain in weight. With the presence of infiltrated SiO_2 as a bond phase oxidation weight gain decreased from 8.73 to 2.02%; bulk density, flexural strength and young modulus increased from 1.83 to 2.10 gm/c^3, 29.47 to 47.88 MPa and 27.56 to 41.28 GPa, respectively with decrease in porosity from 35.59 to 26.12 vol.%. Fig. 8(b) shows the XRD results of the SBSC ceramics and it contained only SiC and cristobalite as crystalline phases. The firing shrinkage in case of SBSC specimens was observed to be very negligible which meant that the introduction of SiO_2 via the pyrolysis of precursor oxide network did not alter SiC particle network. The SiC particles were connected by crystalline SiO_2 bonds at the contacting points and their network structure was stabilized. The accumulation of silica resulted in increase in density and

Table 1
Effect of SiO_2 infiltration on characteristics of porous SiC ceramics.

Type of the sample	% of mass increase	% of wt. gain after firing	Bulk density (g/cm^3)	Porosity (%)	Flexural strength (MPa)	Young's Modulus (GPa)
SiC ceramics made without infiltrated SiO_2	–	8.73 ± 1.28	1.83 ± 0.02	35.59	29.47 ± 2.40	27.56 ± 2.09
SiC ceramics made with infiltrated SiO_2	21.01 ± 0.72	2.02 ± 0.80	2.10 ± 0.07	26.12	47.88 ± 3.63	41.48 ± 4.69

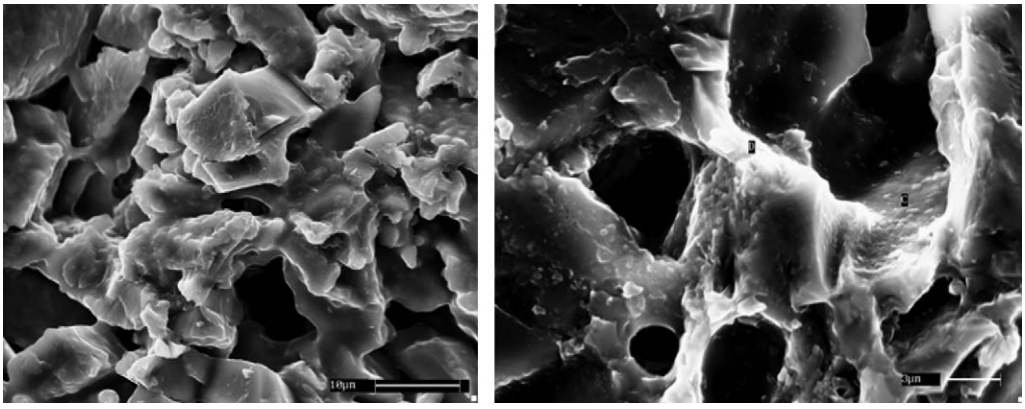

Fig. 9. SEM images of SBSC specimens – (L) formation of SiO_2 bonds connecting the neighbouring SiC particles at the contacting points and (R) crystalline silica bridging SiC particles.

decrease in porosity. SiC particles originally contained a very thin surface oxide layer [34]. During SiO_2 sol infiltration colloidal particles might have interacted with the surface oxide layer. In the subsequent solvent removal stage a continuous network of condensed oxide phase appeared to have formed which finally could result in formation of SiO_2 layer on SiC particle surface. The SiO_2 layer acted as a protective scale putting severe restriction to oxidation [35] causing significantly low oxidation weight gain. Scanning electron microstructural images clearly showed formation of SiO_2 bonds at regions of contacting SiC particles (Fig. 9(a)) and well developed necks between SiC particles were clearly observed (Fig. 9(b)). EDX analysis showed the presence of crystalline SiO_2 in the bond phase. Formation of SiO_2 bond caused improvement of mechanical properties for SBSC specimens.

Mercury porosimetry results of SBSC and SiC samples prepared without infiltrated silica are compared in Fig. 2. Broad distribution patterns were obtained which might be due to wide variation of starting SiC powder sizes. A maximum pore size of around 7 μm was obtained in case of SiC samples processed without addition of infiltrated silica. Two peaks one at 17 nm and other at 5 μm were obtained for SBSC specimens with an average pore size of 4.56 μm. Pores of nanometer sizes were most likely present in the crystalline SiO_2 bond phase. Pore size distribution was also determined during microstructural examination under SEM following image analysis method with the help of standard software (Leica Q 500MC). The data are presented in Fig. 10 which indicates an average pore size of 4.07 μm. The results of the pore size distribution obtained from Hg-porosimetry test and image analysis method showed close agreement.

SBSC specimens showed improvement in mechanical properties compared to its counterpart processed without infiltrated SiO_2. Porosity plays an important role in determining the mechanical strength of porous ceramics. Flexural strength decreases as porosity increases and the strength–porosity relationship bears an exponential dependence [36]. Size of the pores also can exert a negative influence on strength [37]. In case of oxidation bonded SiC ceramics She et al. showed that the strength at a given porosity is determined mainly by the size of the oxide neck rather than the starting SiC particle size [15]. In the context of reported information it appears that the high strength of 48 MPa obtained in the present study is related to decreased porosity and larger neck size expectedly caused by the more addition of infiltrated SiO_2.

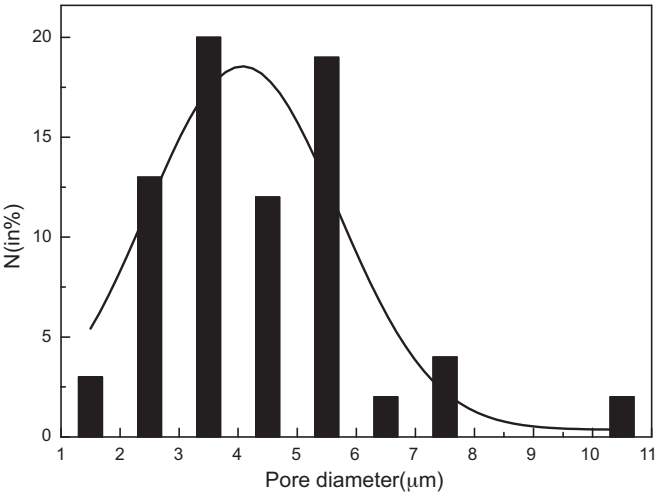

Fig. 10. Pore size distribution pattern of SBSC ceramics obtained from micrographs by image analysis method.

4. Conclusion

Synthesis of porous SiC ceramics was demonstrated by an infiltration technique consisting of intrusion of silica sol as a liquid SiO_2 precursor into SiC powder compacts followed by heat treatment at 1300 °C in air. Infiltration of the liquid precursor into SiC powder compacts occurred in two steps, viz., an initial rapid infiltration of the precursor governed by capillary pressure and a slow impregnation via diffusion. Both steps were controlled by parabolic rate laws. The extent of infiltrated silica was found to be dependent on the number of infiltration passes. The final material exhibited the presence of cristobalite after firing at 1300 °C which was believed to act as a bond between the neighboring SiC particles at the contacting points. The presence of cristobalite in the porous compact resulted in a material with a reasonable flexural strength at usable levels of porosity and pore size.

Acknowledgements

The authors would like to thank Mr. A. Seal of Sensor and Actuator Division, CGCRI, for his help in doing the rheological analysis. We are also grateful to Mr. S.K. Dalui, Mechanical Property Evaluation Section, for his help in doing mechanical characterization, Mrs. M. Majumder, Instrumentation Division, for her help in thermal analysis and pore size distribution determination test and Mr. S. Roy, Electron Microscopy Section, for carrying out microscopic examination. One of the authors (A. Dey) expresses grateful appreciation to CGCRI (CSIR) for its support to him by offering Project Assistantship under Supra Institutional Project (SIP0023).

References

[1] M. Benaissa, J. Werckmann, G. Ehret, E. Peschiera, J. Guille, M.J. Ledoux, Structural studies of active carbon used in the growth of silicon carbide catalyst support, J. Mater. Sci. 29 (1994) 4700–4707.
[2] N. Keller, C. Pham-Huu, S. Roy, M.J. Ledoux, C. Estournes, J. Guille, Influence of the preparation condition on the synthesis of high surface area SiC for use as a heterogeneous catalyst support, J. Mater. Sci. 34 (1999) 3189–3202.
[3] P.H. Pastila, V. Helanti, A.P. Nikkila, T.A. Mantyla, Effect of crystallization on creep of clay bonded SiC filters, Ceram. Eng. Sci. Proc. 19 (1998) 37–44.
[4] M. Fukushima, Y. Zhou, Y. Yoshizawa, Fabrication and microstructural characterization of porous SiC membrane supports with Al_2O_3–Y_2O_3 additives, J. Membr. Sci. 339 (1–2) (2009) 78–84.
[5] C. George Wei, T.N. Oak. Ridge, Method for forming fibrous silicon carbide insulating material, US Pat. No. 4481179 (6 November 1984).
[6] A. Vonsivici, G.T. Reed, A.G. Evans, (-SiC- on insulator waveguide structures for modulators and sensor systems, Mater. Sci. Semicon. Proc. 3 (2000) 367–382.
[7] S.H. Kim, Y.-W. Kim, J.-Y. Yun, H.D. Kim, Fabrication of porous SiC ceramics by partial sintering and their properties, J. Kor. Ceram. Soc. 41 (2004) 541–546.
[8] Y.-W. Kim, S.-H. Kim, I.-H. Song, H.-D. Kim, C.B. Park, Fabrication of open-cell microcellular silicon carbide ceramics by carbothermal reduction, J. Am. Ceram. Soc. 88 (10) (2005) 2949–2951.
[9] J.-H. Eom, Y.-W. Kim, I.-H. Song, H.-D. Kim, Microstructure and properties of porous silicon carbide ceramics fabricated by carbothermal reduction and subsequent sintering process, Mater. Sci. Eng. 464 (2007) 129–134.
[10] I.-K. Sung, S.-B. Yoon, J.-S. Yu, D.-P. Kim, Fabrication of macro porous SiC from templated preceramic polymers, Chem. Commun. (2002) 1480–1481.
[11] X.W., D.L. Jiang, J.H. She and S.H. Tan, Preparation and characterization of porous SiC based ceramics, D.S.Yan, Z.D.Guan (Eds.), Proceedings 1st China International Conference on High Performance Ceramics, October, 1998, Beijing, pp. 266–269.
[12] X. Zhu, D. Jiang, S. Tan, Improvements in the structure of reticulated porous ceramics by vacuum degassing, Mater. Lett. 51 (2001) 363–367.
[13] Y. Ma, Q.-S. Ma, J. Suo, Z.-H. Chen, Low temperature fabrication and characterization of porous SiC ceramics using silicone resin as binder, Ceram. Intl. 34 (2) (2008) 253–255.
[14] S. Zhu, S. Ding, H. Xi, R. Wang, Low temperature fabrication of porous SiC ceramics by preceramic polymer reaction bonding, Mater. Lett. 59 (2005) 595–597.
[15] J.-H. She, Z.Y. Deng, J.D. Doni, T. Ohji, Oxidation bonding of porous silicon carbide ceramics, J. Mater. Sci. 37 (2002) 3615–3622.
[16] J.-H. She, J.F. Yang, N. Kondo, T. Ohji, S. Kanazaki, Z.-Y. Deng, High strength porous silicon carbide ceramics by an oxidation-bonding technique, J. Am. Ceram. Soc. 85 (11) (2002) 2852–2854.
[17] J.-H. She, T. Ohji, Porous mullite ceramics with high strength, J. Mater. Sci. Lett. 21 (2002) 1833–1834.
[18] S. Ding, S. Zhu, Y.-P. Zeng, D. Jiang, Fabrication of mullite bonded porous silicon carbide ceramics by in situ reaction bonding, J. Euro. Ceram. Soc. 27 (4) (2007) 2095–2102.
[19] N. Bardhan, P. Bhargava, In situ reaction sintering of porous mullite bonded silicon carbide. Its mechanical behavior and high temperature application, Ceram. Eng. Sci. Proc. 29 (2008) 127–140.
[20] S. Liu, Y.-P. Zeng, D. Jiang, Fabrication and characterization of cordierite bonded porous silicon carbide ceramics, Ceram. Int. 35 (2) (2009) 597–602.
[21] K. Morimoto, K. Inoue, S. Kawasaki and H. Sakai, Honeycomb structure, US pat. No. 6815038 (9 November 2004).
[22] F. Zok, F.F. Lange, J.R. Porter, Packing density of composite powder mixtures, J. Am. Ceram. Soc. 74 (8) (1991) 1880–1885.
[23] F.F. Lange, L. Atteraas, F. Zok, J.R. Porter, Deformation consolidation of metal powders containing steel inclusions, Acta Metall. Mater. 39 (1991) 209–219.
[24] B. Karmakar, G. De, D. Ganguli, Dense silica microspheres from organic and inorganic acid hydrolysis of TEOS, J. Non-cryst. Sol. 272 (2–3) (2000) 119–126.
[25] B. Karmakar, G. De, D. Ganguli, Silica microspheres from the system tetraethyl orthosilicate-acetic acid-water, J. Non-cryst. Sol. 135 (1991) 29–36.
[26] J. Contantz, W.N. Herkelrath, F. Murphy, Air encapsulation during infiltration, Soil Sci. Soc. Am. J. 5 (1988) 10–16.
[27] W.C. Tu, F.E. Lange, Liquid precursor infiltration processing of powder compacts: I,Kinetic studies and microstructure development, J. Am. Ceram. Soc. 78 (12) (1995) 3277–3288.
[28] F.A. Dullien, Porous media-fluid transport and pore structure, Academic Press, New York, 1979.
[29] G.H. Geiger, D.R. Parier, Transport phenomena in metallurgy, Addison-Wesley, New York, 1980.
[30] H. Yu, C. Lu, T. Xi, L. Luo, J. Ning, C. Xiang, Thermal decomposition of the carbon nanotube/SiO_2 precursor powders, J. Therm. Anal. Calorim. 82 (2005) 97–101.
[31] C.M. Whang, C.S. Yeo, Y.H. Kim, Preparation and characterization of sol–gel derived SiO_2–TiO_2–PDMS composite films, Bull. Korean Chem. Soc. 22 (12) (2001) 1367–1370.
[32] G.M. Anilkumar, U.S. Hareesh, A.D. Damodaran, K.G.K. Warrier, Effects of seeds on the formation of sol–gel mullite, Ceram. Int. 23 (1997) 537–543.
[33] A.M. Menchi, A.N. Scian, Mechanism of cordierite formation obtained by sol–gel technique, Mater. Lett. 59 (2005) 2664–2667.

[34] M.A. Mulla, V.D. Krstic, Low temperature pressureless sintering of β-silicon carbide with aluminum oxide and yttrium oxide additions, Am. Ceram. Soc. Bull. 70 (1991) 439–443.
[35] E.A. Gulbransen, S.A. Janson, High temperature oxidation, reduction and volatalisation reactions of silicon and silicon carbide, Oxid. Metals 4 (3) (1972) 181–201.
[36] M.F. Ashby, The mechanic properties of cellular solids, Metall. Trans. 14A (1983) 1755–1769.
[37] D.M. Liu, Influence of porosity and pore size on the compressive strength of porous hydroxyapatite ceramic, Ceram. Int. 23 (2) (1997) 135–139.